Analytical Methods

ROYAL SOCIETY OF CHEMISTRY

PAPER

View Article Online
View Journal | View Issue

Cite this: *Anal. Methods*, 2021, **13**, 1286

Flexible paper-based label-free electrochemical biosensor for the monitoring of miRNA-21 using core–shell Ag@Au/GQD nano-ink: a new platform for the accurate and rapid analysis by low cost lab-on-paper technology†

Fatemeh Farshchi,‡[a] Arezoo Saadati,‡[b] Nazanin Fathi,[c] Mohammad Hasanzadeh *[a] and Mohammad Samiei*[d]

miRNA-21 is one of the most famous and prominent microRNAs that is important in the development and emergence of cancers. So, the sensitive and selective monitoring of miRNA-21 as a very common biomarker in cancer treatment is necessary. In this work, a novel paper-based electrochemical peptide nucleic acid (PNA) sensor was developed for the detection of miRNA-21 in human plasma samples by using Ag@Au core–shell nanoparticles electrodeposited on graphene quantum dots (GQD) conductive nano-ink (Ag@Au core–shell/GQD nano-ink), which was designed directly by writing pen-on paper technology on the surface of photographic paper. This nano-ink has a great surface area for biomarker immobilization. The prepared paper-based biosensor is very small and cheap, and also has high stability and sensitivity. Hybridization of PNA was measured using various electrochemical techniques, such as cyclic voltammetry (CV), square wave voltammetry (SWV) and chronoamperometry (ChA). FE-SEM (Field Scanning Electron Microscope), TEM (Transmission Electron Microscope), EDS and DLS (Dynamic Light Scattering) tests were performed to identify the engineering safety sensor. Under optimal conditions, the linear range for the calibration curve was from 5 pM to 5 μM, and the achieved LLOQ was 5 pM. The obtained results recommended that the proposed bioassay might be suitable for an early diagnosis of cancer based on the inhibition of the expression of miRNA-21, which activates the enzyme caspase and accelerates apoptotic proteins and death in tumor cells.

Received 26th January 2021
Accepted 30th January 2021

DOI: 10.1039/d1ay00142f

rsc.li/methods

1. Introduction

Recent research has shown that miRNAs (small non-coding endogenous RNA) can serve as a biomarker for the timely detection of cancers,[1–3] and it is interesting to note that, unlike other RNAs, they are highly stable under *in vivo* and *in vitro* conditions. miRNAs are non-coding ribonucleic acids that are evolutionarily protected. miRNAs are short single-stranded sequences of about 18 to 25 nucleotides in size.[4,5] The main function of miRNAs is in post-transcriptional regulation. miRNAs complement a portion of one or more messenger RNAs.[5] These molecular structures participate in physiological and pathological cell processes, and many of them can act as oncogenes or tumor inhibitors. Therefore, mutations in these open reading molds can lead to cancer. Recently, the number of studies examining miRNAs as biomarkers of malignancies in tissue samples has increased dramatically. About 15 miRNAs can differentiate between cancerous and normal tissue.[4,6] miRNA-21 is one of the most famous and prominent microRNAs that is important in the development and emergence of cancers. Inhibition of the expression of this miRNA activates the enzyme caspase, and accelerates apoptotic proteins and death in tumor cells. In malignancies, such as glioblastoma, breast cancer, hepatocellular carcinoma, and gastric cancer, an increase in miRNA-21 has been reported in tissues. Elevated serum miRNA-21 has also been reported in many malignancies, such as ovarian cancer, lung cancer, liver cell carcinoma, laryngeal cancer and lymphoma, making this microRNA a very common biomarker in cancer treatment.[7–9] Quantitative polymerase chain reaction (qPCR) is commonly used to measure miRNAs,

[a]*Pharmaceutical Analysis Research Center, Tabriz University of Medical Sciences, Tabriz, Iran. E-mail: hasanzadehm@tbzmed.ac.ir*

[b]*Food and Drug Safety Research Center, Tabriz University of Medical Sciences, Tabriz, Iran*

[c]*Research Center for Immunodeficiencies, Pediatrics Center of Excellence, Children's Medical Center, Tehran University of Medical Sciences, Tehran, Iran*

[d]*Faculty of Dentistry, Tabriz University of Medical Sciences, Tabriz, Iran. E-mail: samiei.moh@gmail.com*

† Electronic supplementary information (ESI) available. See DOI: 10.1039/d1ay00142f

‡ Co-first author.

which requires advanced equipment and specialists, and is time consuming and expensive.[10–14]

In recent years, biosensors have received a great deal of attention for the detection and identification of biomarkers and miRNAs. These devices are based on the integration of a biological and transducer element, and can be said to complement ELISA and PCR techniques. So far, several optical and electrochemical biosensors have been developed to detect miRNAs. For example, Peng and colleagues[14] have developed a SERS biosensor for the detection of miRNA-10b. Joshi *et al.*[15] designed a SPR biosensor to identify miRNA-10b and miRNA-21 using AuNPs, which had an extraordinary diagnostic limit. On the other hand, electrochemical biosensors have attracted special attention due to their great ability to work in complex samples, such as blood or urine, and the ability to shrink for use in microfluidics.[16] Besides the DNA-oligonucleotide, peptide nucleic acid (PNA) is currently used as an ingredient bio-active in the designing of the biosensors.[17] PNA is a DNA analog, which is capable of pairing with DNA or RNA, according to the Watson–Crick model.[18] Compared to DNA oligonucleotides, PNA has better properties, such as higher chemical stability and more sensitivity in high temperatures. The PNA structure includes a *N*-(2-aminoethyl) glycine motif and four natural nucleobases that are linked together by a methylene carbonyl group. PNA is load-free, which increases the resistance between PNA/DNA and PNA/RNA bonds. All of these features make the PNAs a good option in the identification of miRNAs.[19] Therefore, the detection of miRNAs by PNA-based biosensors can be a great help in the rapid and timely detection of many cancers.[20]

Providing quantitative analysis information without the need for additional processing steps and at high speeds is required. In this regard, microfluidic paper-based biosensors have become a new and powerful technology as a novel and convenient technology with low cost and easy portability.[21] These biosensors have included one or numerous layers of paper, and have hydrophilic paper channels that are designed by hydrophobic materials.[21] With this technique, the concentration of different liquids, such as urine, blood or serum, can be determined independently for different types of analytical and measurement experiments.[22] Paper-based biosensors are a new type of biosensors that are very low cost and also very easy to transport. These biosensors have one or more hydrophilic paper layers that are designed by hydrophobic materials, and can hold different liquids. They can analyze human blood, serum, or urine in various concentrations in one or two steps accurately and quickly.[23] Electrochemical paper-based biosensors are very good methods due to their high accuracy and sensitivity. These sensors can shrink. In addition, their cost of design and construction is very low, so they can be a powerful tool in cancer treatment.[24] Paper can be a very good substrate for electrochemical biosensors due to its high flexibility and high electrical resistance, and it can be so helpful in point-of-care testing.[25] Paper-based biosensors with applied inks containing metal nanoparticles are an excellent choice for use in paper biosensors due to their high conductivity and biocompatibility, as well as low toxicity.

Carbon inks and metal nanoparticles have good properties, such as excellent conductivity, low toxicity, easy access, cheap and biocompatible. So, conductive inks have been widely used in the design of paper-based biosensors.[26] Inks containing metal nanoparticles, such as AgNPs and AuNPs, have high electrical conductivity. They are suitable and have good oxidation stability. So, they can be used as a powerful element in electrical paper-based biosensors.[27,28] Conductive nanocomposites have particular importance in the engineering of paper-based electrochemical biosensors due to their sensitivity and stability.[29]

In this work, we developed a novel paper-based electrochemical PNA sensor for the detection of miRNA-21 using Ag@Au core–shell/GQD nano-ink. The prepared biosensor was simple, affordable, and also has an acceptable linear range. FE-SEM (Field scanning Electron Microscope), TEM (Transmission Electron Microscope), EDS and DLS (Dynamic Light Scattering) tests were performed to identify the engineering of the safety sensor.

2. Materials and methods

2.1 Reagents and chemicals

The oligonucleotide sequences were purchased from Takapouzist Co. (Iran). All of the target oligonucleotides used in this study were synthesized and purified through BioRP by Bionner Co. (Korea).

- The acpcPNA-T9 probe′: TTTTTTTTTLysNH$_2$
- miRNA-21: 5′-rUAGCUUAUCAGACUGAUGUUGA-3′

miRNA-21 oligonucleotides were diluted with 0.1 M Tris–HCl buffer (pH ~7.4). Trisodium citrate ($C_6H_5O_7Na_3 \cdot 2H_2O$), $AgNO_3$, polyvinylpyrrolidone (PVP), sodium borohydride ($NaBH_4$), hydrogen peroxide (H_2O_2), triethylamine ($C_6H_{15}N$), acetic acid (CH_3COOH), potassium iodide (KI), hydrogen tetrachlorocuprate (III) hydrate ($HAuCl_4 \cdot 3H_2O$), citric acid ($C_6H_8O_7$), chitosan ($C_6H_{11}NO_4$), MCE (mercaptoethanol), NaOH (sodium hydroxide), graphite, ethylene glycol ($C_2H_6O_2$), ethanol (C_2H_5OH), potassium ferricyanide ($C_6N_6FeK_3$), potassium ferrocyanide ($C_6FeK_4N_6$) and potassium chloride (KCl) were obtained from Sigma Aldrich (Ontario, Canada). The supporting electrolyte for electrochemical analysis was 0.01 M of $[Fe(CN)_6]^{3-/4-}$. Human plasma samples were obtained from the Iranian Blood Transfusion Research Center (Tabriz, Iran).

2.2 Instruments

All of the electrochemical measurements were carried out using a portable potentiated Palm Sense 4c (Palm Instruments, Utrecht, The Netherlands) connected to a laptop by PS Trace software. The prepared paper with synthesized ink (Ag@Au core–shell/GQD nano-ink) was tested as a three-electrode system (working electrode, a reference electrode and counter electrode). FE-SEM (high-resolution field emission scanning electron microscope), Hitachi SU8020, Czech with a 3 kV effective voltage was used for investigating the morphology of the electrode surface. Energy scattering spectroscopy (EDS) was used to study the chemical combination. A transmission electron microscope (TEM, Philips CM30 electron microscope) was employed to investigate the mechanism of synthesis. DLS

(Dynamic Light Scattering) with the zeta potential instrument Malvern Instruments Ltd (Zetasizer Ver. 7.11, MAL1032660, England) was employed for studying the size-frequency and zeta potential of the synthesized ink.

2.3 Synthesis of the Ag@Au core shell

Ag nanoprisms (Ag NPr) were prepared and defined according to our previous works.[16] To prepare the Ag@Au core–shell nanoparticles, at the first step, a mixture containing PVP (40 μl, 5% w) with KI (80 μl, 0.2 M) and $HAuCl_4$ (20 μl, 0.25 M) was combined with 9 ml of H_2O. In the second step, PVP (1 ml, 5% w) was combined with triethylamine (150 μl) and ascorbic acid (200 μl, 0.5 M). Then, 1 ml of the prepared solution was mixed with 1 ml of AgNPs. Finally, 1.2 ml of the first stage solution was added to the second stage solution, centrifuged at 8000 rpm for half an hour, and washed three times with distilled water (DW) to remove excess reactants. We expelled the surface solution, and use its sediment in the preparation of the conductive nano-ink.

2.4 Synthesis of Ag@Au core–shell/GQD conductive nano-ink

GQD was synthesized according to our previous works.[30,31] For the synthesis of the conductive nano-ink, 0.013 g of chitosan was dissolved in 2 ml of acetic acid (0.1 M). Then, 0.2 g of PVP, 0.6 g of graphite and the Ag@Au core–shell NPs were magnetically mixed. Then, 2 ml of GQDs was added and magnetically stirred for about 20 min. Finally, the prepared solution was incubated for 12 hours at 60 °C. After 12 hours, the prepared solution was placed at 80 °C, and 500 μl of sodium hydroxide (8 M) was added drop by drop. Then, it was centrifuged for 30 minutes (8000 rpm). After washing for 3 times, the prepared nano-ink was mixed with ethanol, DW and ethylene glycol in a ratio of 6 : 3 : 6 ml and sonicated for 30 minutes (Fig. S1 (see ESI†)).

2.5 Conductivity study of the Ag@Au core–shell/GQD conductive nano-ink

To test the conductivity of the synthesized nano-ink, we drew various shapes and lines in different diameters on the surface of the photographic and ivory sheet papers. We then placed a battery (3.0 V) and a LED (3.0 V) on the surface of the paper with a conductive wire. The cathode part of the battery was attached on the surface of the lines, and the anode part of the battery was fixed to the lamp (Fig. 1). When the current flows from the anode to the cathode, an electrical circuit is created and the LED lamp turns on. We also used ohmmeters to check the resistance of the conductive lines, which is shown in Fig. 1. According to Fig. 2, the flexibility of the conductive lines was ensured by bending the paper.

2.6 Characterizations

2.6.1 Characterization of the Ag@Au core–shell/GQD nano-ink. TEM imaging was applied to evaluate the size, morphology and confirmation of the Ag@Au nanoparticles binding to the graphite sheets. The particles are visible in a spherical shape. Ag is at the core, and Au surrounds it like a shell. QDs nanoparticles are also visible on the plates. To study the morphology of the synthesized ink, FE-SEM imaging was used. As shown in Fig. 3, a bulk and uniform structure of the graphite sheets has been shown in which the Ag@Au core–shell NPs are finely placed on graphite sheets (more FESEM images can be seen in Fig. S1 (see ESI†)). According to Fig. 3, the EDS spectrometer has also been used for elemental analysis. It is clear that carbon is present in large quantities. The presence of Au and Ag nanoparticles in the structure of the synthesized ink is also quite evident. DLS (dynamic light scattering) was used to measure the particle size distribution and charge. This technique is a simple,

Fig. 1 Photographic demonstration of the patterns with various thicknesses prepared with Ag@Au core–shell/GQD nano-ink on the surface of the ivory sheet and photographic paper.

Fig. 2 Display of the flexibility of the Ag@Au core–shell/GQD nano-ink drawn on the surface of the photographic paper.

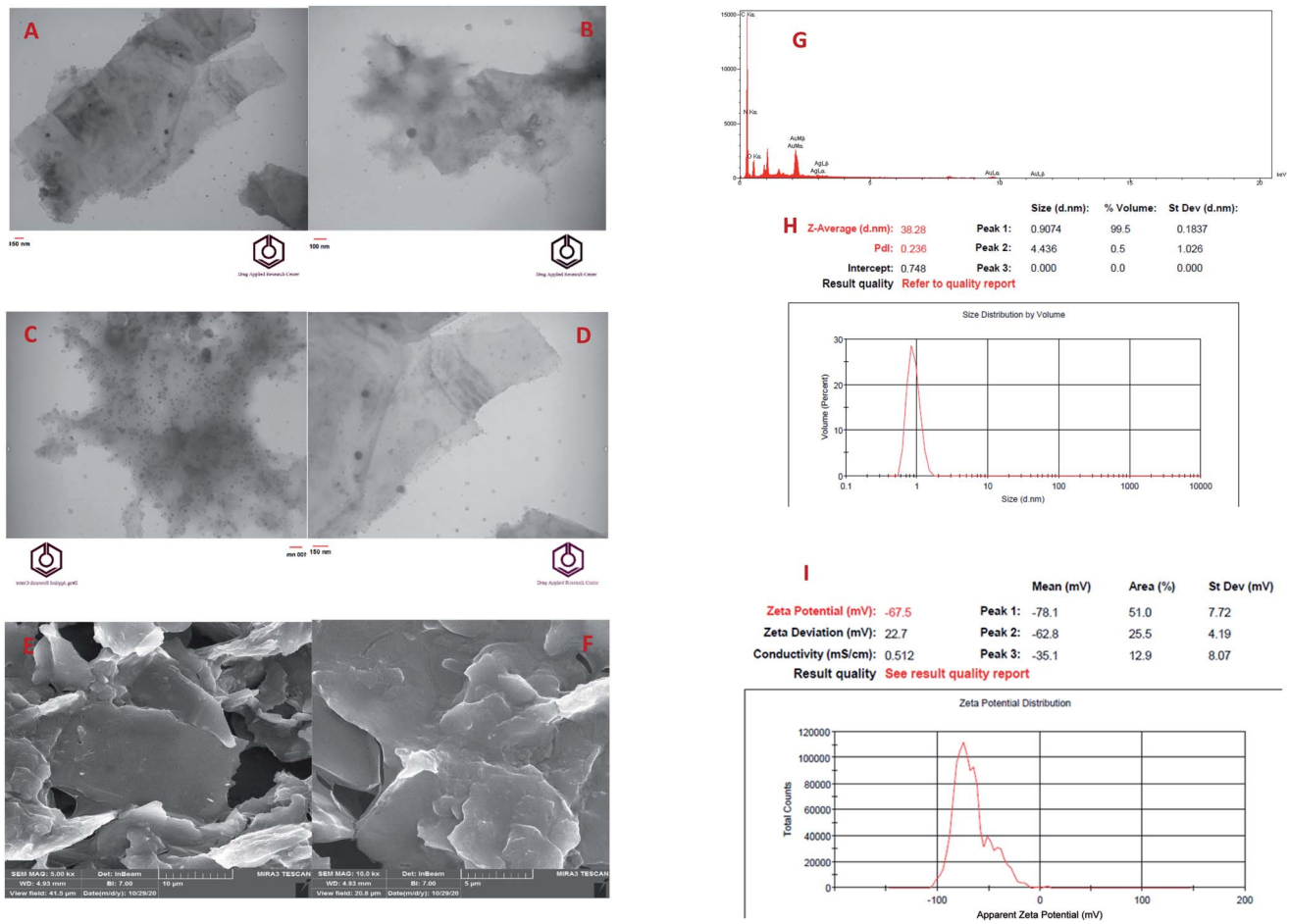

Fig. 3 (A–D) TEM images of the prepared Ag@Au core–shell/GQD nano-ink. (E and F) FE-SEM images of the prepared nano-ink in different exaggerations. (G) EDS images of the bulk Ag@Au core–shell/GQD nano-ink. (H) Size distribution analysis of the Ag@Au core–shell/GQD nano-ink by DLS. (I) Recorded Zp for synthesized Ag@Au core–shell/GQD nano-ink.

inexpensive and reproducible method that is widely used to measure the particle size and surface charge. As shown in Fig. 3H, the nanoparticle distribution range is 0–10 nm. The zeta potential is very important for understanding and controlling the properties of the colloidal suspensions. Generally, the properties of a suspension can be identified by understanding how the colloids interact with each other. By changing the balance between the repulsive forces and gravity between the particles, the viscosity of the solution can be changed and adjusted. Many substances exhibit varying degrees of the zeta potential when exposed to liquids or water. Also, water molecules in the vicinity of the cell membrane are almost immobile, and their presence with charged groups on the membrane surface affects the release of mobile ions. The membrane surface of the isolated cells is usually negatively charged. The equilibrium of dissociation and protonation is strongly dependent on the pH value of the liquid medium. Therefore, it has a strong influence on the formed surface charge of the material and further on the zeta potential. On inert surfaces, the negative surface charge is formed due to the preferential adsorption of hydroxide ions from water. Inert surfaces are thus negatively charged at neutral and alkaline pH. As shown in Fig. 3I, the zeta potential is negative (−67.5). Saeb *et al.* showed that particles with zeta potential values more than +30 mV or more than −30 mV have good stability.[32] Also, if the amount of the zeta potential increases, the aggregation decreases and the size of the nanoparticles becomes larger.[33] Therefore, the negative zeta potential values showed that the synthesized nanocomposite has good stability (please see more FESEM and TEM images in Fig. S2 (ESI†)).

2.6.2 FE-SEM and EDC of various steps of the prepared paper-based biosensor. The step-by-step morphology of the biosensor preparation was imaged by FE-SEM (Fig. S4A–O†). First, the images of the synthesized nano-ink were recorded on the surface of the photographic paper. According to the images (Fig. S3A–E (see ESI†)), it is clear that the graphite sheets have created an uneven surface. After incubation of PNA-T9 (Fig. S4F–J†) and miRNA-21 (Fig. S4K–O†), the morphology has completely changed and the surface roughness has increased, indicating the successful stabilization of the biological material on the surface of the paper (please see more FESEM images in Fig. S4 (ESI†)). According to the EDS spectroscopic images, a large amount of carbon is related to the nano-pattern on the photographic paper and the amount of

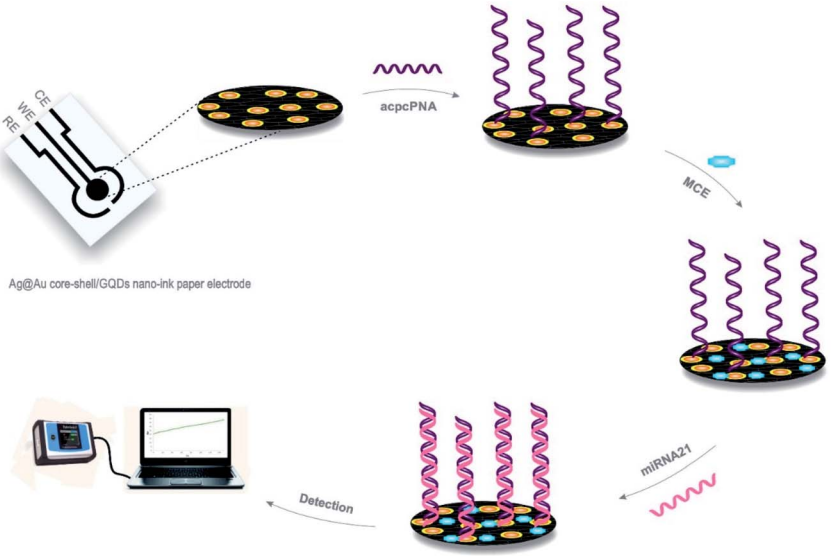

Scheme 1 Preparation of the PNA-based electrochemical biosensor for the detection of miRNA-21 on the surface of the photographic paper.

AgNPs and AuNPs related to the Ag@Au core–shell NPs, and indicates the successful synthesis. In the later stages, the amount of P is increased, which is related to the incubation of biological materials on the surface of the prepared electrode. In this step, the amount of AgNPs has decreased. It seems that the amount of silver is overshadowed by the addition of biological materials.

2.7 Preparation of the paper-based electrochemical PNA sensor

To prepare the electrochemical paper-based electrode, the synthesized Ag@Au core–shell/GQD nano-ink was designed on the surface of the paper using a mask and dried at room temperature for 5 minutes. Then, 5 μl of PNA-T9 was drop-casted on the sensor area of the paper-based electrode and incubated for

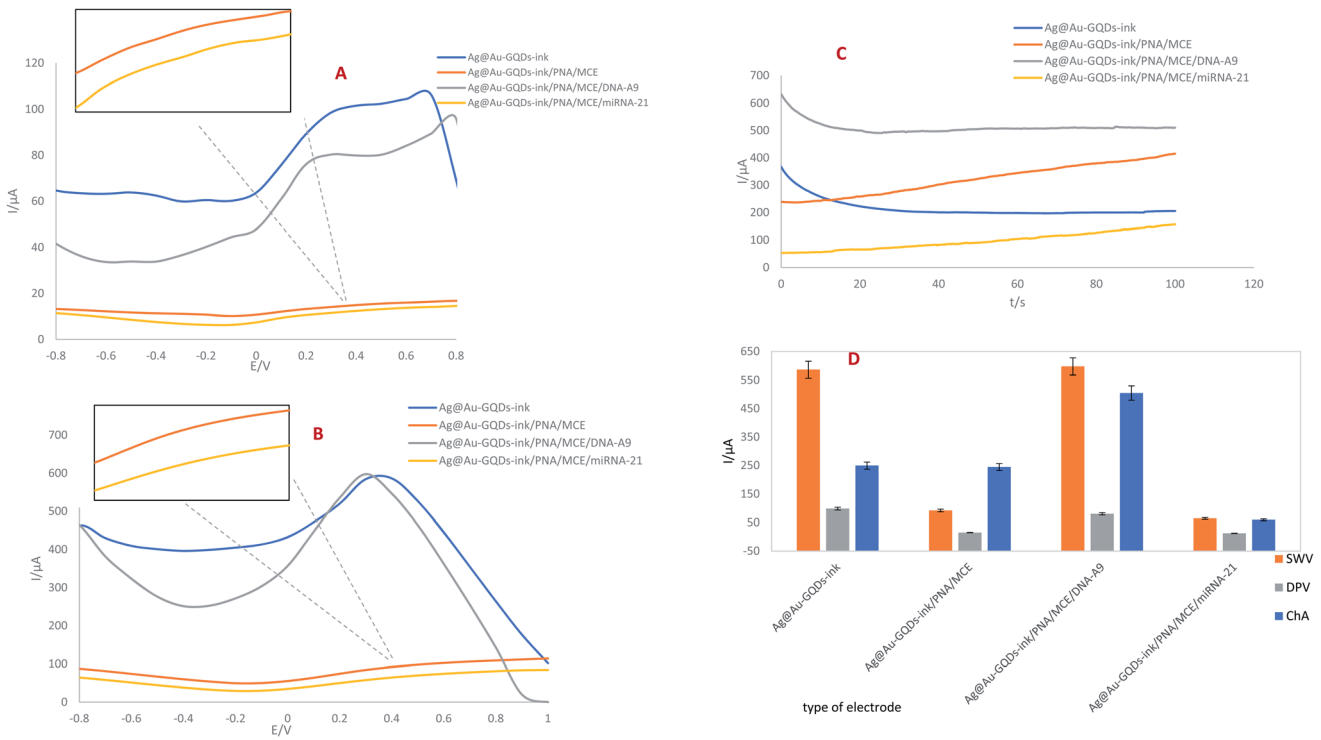

Fig. 4 (A) DPVs (step potential = 1.0 V, E_{pulse} = 0.1, t_{pulse} = 0.2 s, and scan rate = 10 mV s^{-1}). (B) SWVs (stop potential = 0.1 V, frequency = 1.0 Hz). (C) ChAs (E = 0.5 V, duration = 150 s) of various steps of the prepared PNA-based biosensor on the surface of photographic paper in 0.01 M $[Fe(CN)_6]^{3-/4-}$/KCl solution as the supporting electrolyte. (D) Histogram of the peak current against the type of electrode (n = 3, SD = 1.86).

12 hours at 4 °C. MCE was used as a biological antioxidant to prevent the detected sites and increase the PNA-T9 affinity. Finally, miRNA-21 was dropped on the electrode surface, and then examined by various electrochemical techniques. It is necessary to mention that after all incubation stages, the surface of the electrodes was washed in Tris buffer solution. Scheme 1 shows the preparation steps of the electrochemical PNA-based biosensor.

3. Results and discussion

3.1. Electrochemical performance of the prepared biosensor in different steps

The electrochemical performance at different stages was investigated using various biochemical techniques (DPV-SWV and ChA) in 0.01 M $[Fe(CN)_6]^{3-/4-}$/KCl (Fig. 4). Considering the high current intensity, which is equal to 250 μA in ChA, 100 μA in DPV and 590 μA in SWV technique, it can be proved that the synthesized ink has a suitable surface area. The nanoparticles on the surface of the photographic paper also act as anchors for the thiol groups, and effectively speed up the electron transfer by $[Fe(CN)_6]^{3-/4-}$/KCl solution. It can also provide a suitable substrate for probe incubation. MCE also acts as an insulator and reduces the speed of electron transfer, so the intensity of the currents has significantly reduced. After DNA-A9 incubation, due to the complementary binding to the probe bases (PNA-T9), the electron transfer rate increased to 500, 80 and 600 μA, respectively. In the last stage after miRNA-21 immobilization on the surface of the PNA-T9/MCE/Ag@Au core–shell/GQD nano-ink paper-based electrode, the electron transfer occurs at a slower speed, so the peak current intensity is reduced.

3.2. Optimization of the miRNA-21 hybridization time

One of the most important factors in evaluating the performance of the PNA-based biosensors is the combination time optimization that shows the connection process between the probe and the target. The appropriate incubation time has a direct effect on the effective duration of the test, and depends on the length of the probe sequence and the nature of the probe. A proper optimal time increases the sensitivity and reproducibility of the biosensor, and reduces the analysis time. In this way, miRNA-21 was incubated at 37 °C in different incubation times (5, 10, 15, 20 and 30 minutes). As shown in Fig. 5, the best incubation time was found by SWV and ChA techniques in 0.01 M $[Fe(CN)_6]^{3-/4-}$/KCl solution as the supporting electrolyte. Based on the obtained results, the maximum peak current was at the 5 minutes incubation, which is approximately 500 μA in SWV and approximately 400 μA in ChA. So, the best time was 5 minutes, and this time was selected.

3.3. Analytical approach

The ChA technique, which is one of the most sensitive electrochemical methods, was used to investigate the effect of the concentration. In this work, different concentrations of miRNA-21 were incubated (37 °C for 10 min) on the surface of the PNA-T9/MCE/Ag@Au core–shell/GQD nano-ink electrode. As shown in Fig. 6, the peak current decreases with decreasing concentration. The calibration curve was obtained by plotting the peak flow logarithm against the miRNA-21 concentration logarithm. The linear range was from 5 pM to 5 μM, and the obtained LLOQ was 5 pM. As shown in Fig. 6B, the standard curves for different concentrations of miRNA-21 were plotted, and the following linear regression equations were gained:

$$\log I_p\ (\mu A) = -0.1283 \log C_{(miRNA\text{-}21)} + 2.7204,\ R^2 = 0.9316.$$

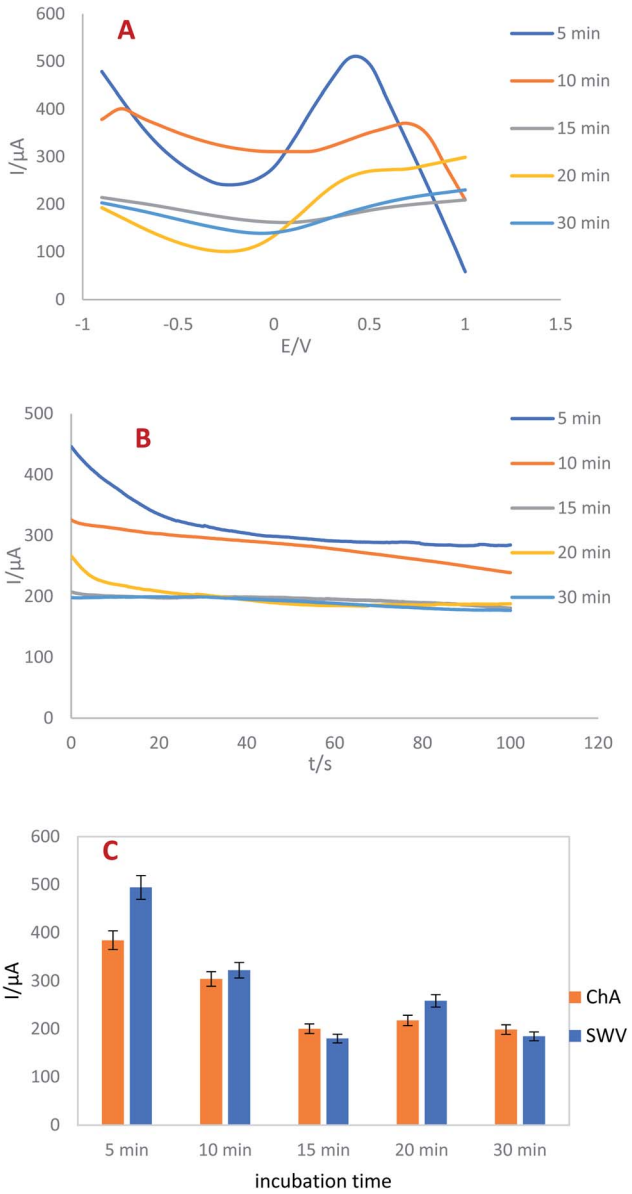

Fig. 5 (A) ChAs ($E = 0.5$ V, duration = 150 s). (B) SWVs (stop potential = 0.1 V, frequency = 1.0 Hz). (C) Histogram of the peak potential and currents of the prepared biosensor after miRNA-21 incubation in various times (5–10–15–20–30 min) on the surface of the photographic paper in 0.01 M $[Fe(CN)_6]^{3-/4-}$/KCl solution as the supporting electrolyte. ($n = 3$, SD = 2.04).

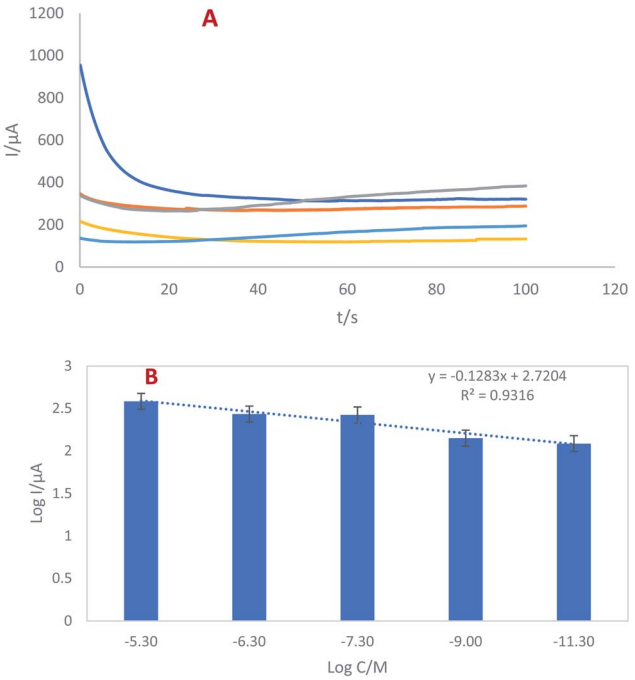

Fig. 6 (A) ChAs of the prepared PNA-based biosensor in different concentrations of target miRNA-21 (5 μM to 5 pM), and (B) calibration curves on the surface of photographic paper in 0.01 M $[Fe(CN)_6]^{3-/4-}$/KCl solution as the supporting electrolyte. (E = 0.5 V, duration = 150 s). (n = 3, SD = 1.46).

The results show the high ability of the prepared paper-based electrochemical PNA-T9 sensor to detect miRNA-21. This biosensor has a simple and easy operation, does not require complex or difficult equipment, and can identify components in a short time. More importantly, it is very small in size; therefore, its transportation is too easy. Due to the good analytical results, compared to previous reports[33–39] (Table S1 [see ESI†]), the designed biosensor has appropriated analytical properties and diagnostic features. Thus, it can be a powerful tool in the clinical laboratories.

Most of the electrochemical methods that are discussed in Table S1† have high analytical power and high selectivity. Compared to the optical biosensors, they have better stability. On the other hand, the prepared PNA based biosensor is label-free. Therefore, its preparation was simple and inexpensive. Due to its small size, its transportation is too easy. Also, this biosensor has a good detection limit and can detect miRNA-21 at low concentration because the nano-ink used has excellent conductivity and unique structural properties. Another important feature of this biosensor compared to other biosensors is the high power of analysis in a short time that can be an alternative to conventional detection methods.[33–39] In general, this biosensor has good analytical properties and is a promising candidate for clinical diagnosis in the future, and can be useful in detecting other biomarkers.

To study the effect of the miRNA-21 concentration in real samples, the prepared plasma was mixed in equal proportions with different concentrations of miRNA-21, and immobilized on the surface of the PNA-T9/MCE/Ag@Au core–shell/GQD nano-ink electrode. Fig. S5 (see ESI†) displays the SWV technique results in different concentrations of microRNAs in human plasma. According to the results, the peak current increases with decreasing concentration. The obtained linear range was from 5 pM to 5 μM, and the obtained LLOQ was 5 pM.

The linear regressions equation obtained from SWV in human plasma samples is as follows:

$$\log I_p\ (\mu A) = -0.1283 \log C_{(miRNA\text{-}21)} + 2.7204,\ R^2 = 0.9316.$$

3.4. Selectivity of the biosensor

The ability to detect similar sequences in oligonucleotide-based biosensors is one of the biggest challenges in designing the biosensor. For this purpose, different mismatch sequences have been used. Various sequences were incubated (5 minutes at 37 °C) on the surface of the prepared electrode mismatches are different in one-base (5′-UAGCUUAUGAGACUGAUGGUUG-3′: MM1) and two-base (5′-UAGCUUAGCGGACUGAUGUUG-3′: MM 2). To evaluate the selectivity of the prepared biosensor, the ChA technique was employed. Fig. 7 shows that in the case of the complementary sequence, the peak current is good, but the peak current was reduced in the presence of mismatches. This

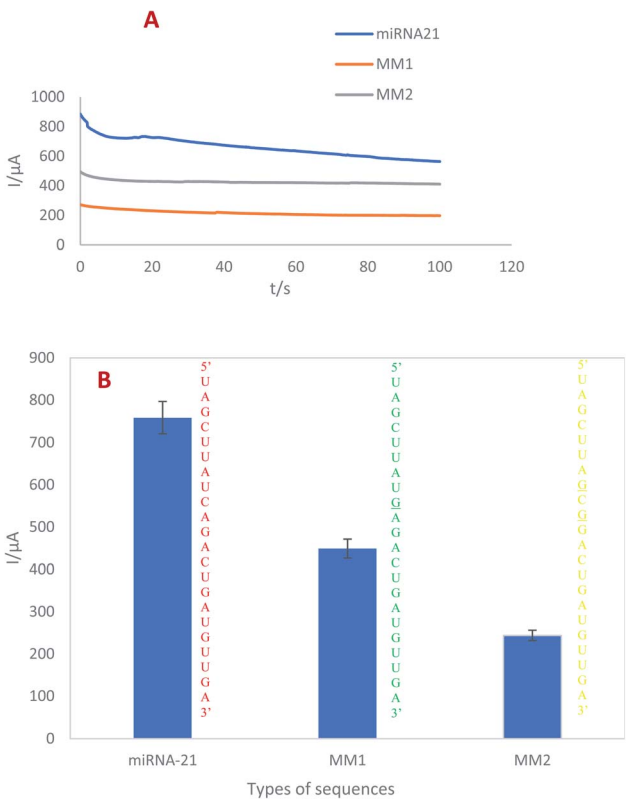

Fig. 7 (A) ChAs of the prepared biosensor for hybridization by target miRNA-21, one-mismatch and two mismatch sequence on the surface of the photographic pfaper. (B) Histogram of the peak potential and currents *versus* of mismatch sequences on the surface of photographic paper in 0.01 M $[Fe(CN)_6]^{3-/4-}$/KCl solution as the supporting electrolyte. (E = 0.5 V, duration = 150 s). (n = 3, SD = 2.51).

is due to the weak hybridization of the mismatches with the PNA-T9 sequence on the surface of the electrode. Given that this biosensor was comprehended as a point of care (not a reference method), it can be said that these changes are insignificant and the designed biosensor has good selectivity.

3.5. Stability and reproducibility of the biosensor

Stability is one of the significant factors in evaluating biosensors for re-use. The stability of PNA on the surface of the prepared biosensor is also important. For this purpose, for 72 hours, the PNA-T9/Ag@Au core–shell/GQD nano-ink on the surface of photographic paper was stored at 4 °C, and the stability of the biosensor was evaluated by using cyclic voltammetry (CV). As shown in Fig. S6 (see ESI†), the performance of the biosensor changes after three days. Therefore, it can be concluded that the biosensor has good performance for 48 hours. Also, to check the repeatability, the performance of three paper electrodes designed with the Ag@Au core–shell/GQD nano-ink was evaluated using the CV method (Fig. S6C (see ESI†)). In general, based on the obtained results, the prepared electrochemical biosensor has good reproducibility and stability.

4. Conclusion

Given that miRNAs can be useful in the early detection of cancer, and the inhibition of the expression of this miRNA activates the enzyme caspase and accelerates apoptotic proteins and death in tumor cells, the early detection of these miRNAs is very important. In this work, for the first time, an electrochemical paper-based biosensor based on PNA-T 9 using conductive nano-ink was developed to detect miRNA-21, which is elevated in most cancers. In this regard, the synthesized Ag@Au core–shell/GQD nano-ink by writing pen-on paper technology was designed on the surface of photographic paper. Compared to the other oligonucleotides, the use of PNA probes increases the stability of the biosensor. Another unique feature of the prepared biosensor is the use of Ag@Au core–shell nanoparticles, which has excellent physicochemical properties. In addition to increasing the stability, it increases the selectivity and sensitivity of the biosensor. The constructed paper-based biosensor can detect miRNA-21 at high speed and accuracy. The linear range for the calibration curve was from 5 μM to 5 pM, and the achieved LLOQ was 5 pM. It also had acceptable results in human plasma samples, so it can be used in complex samples, such as urine or saliva. The rapid and accurate detection of miRNA-21 can prevent many cancerous malignancies, such as glioblastoma, breast cancer, hepatocellular carcinoma and gastric cancer, and prolong the life of patients. According to Table S1,† compared to other biosensors, the proposed bioassay has a good diagnostic limit. Due to the cheap and accessible materials used in the preparation of this biosensor, it can have a great commercial future. On the other hand, this biosensor is easily portable due to its small size, so it can be a powerful tool for quick response to patients and physicians, and reduce the time interval between illness and treatment.

Conflicts of interest

The authors declare that they have no conflict of interest.

Acknowledgements

We gratefully acknowledge the financial support by Tabriz University of Medical Sciences (grant no. 61674). This study was ethically approved (IR.TBZMED.VCR.REC.1397.031) by Tabriz University of Medical Sciences.

References

1 P. Naeli, F. Yousefi, Y. Ghasemi, A. Savardashtaki and H. Mirzaei, *Curr Molecul Med.*, 2020, **20**, 90–101.
2 S. Müller, F. Janke, S. Dietz and H. Sültmann, Circulating MicroRNAs as potential biomarkers for lung cancer, *Tumor Liquid Biopsies*, Springer, 2020, pp. 299–318.
3 N. Fakhri, S. Abarghoei, M. Dadmehr, M. Hosseini, H. Sabahi and M. R. Ganjali, *Spectrochim. Acta, Part A*, 2020, **227**, 117529.
4 V. Nasirian, M. Shamsipur, F. Molaabasi, K. Mansouri, M. Sarparast and V. Salim, *Sens. Actuators B: Chem.*, 2020, **308**, 127673.
5 W. Dai, H. Dong, K. Guo and X. Zhang, *Chem. Sci.*, 2018, **9**, 1753–1759.
6 H. Jia, Y. Bu, B. Zou, J. Wang, S. Kumar and J. L. Pitman, *Analyst*, 2016, **141**, 6297–6302.
7 P. Zhuang, H. Zhang, R. M. Welchko, R. C. Thompson, S. Xu and D. L. Turner, *Sci. Reports.*, 2020, **10**, 1–10.
8 J. Yang, M. Tang, W. Diao, W. Cheng, Y. Zhang and Y. Yan, *Microchim. Acta*, 2016, **183**, 3061–3067.
9 J. Ye, M. Xu, X. Tian, S. Cai and S. Zeng, *J. Pharm. Anal.*, 2019, **9**(4), 217–226.
10 M. Senel, M. Dervisevic, L. Esser, E. Dervisevic, J. Dyson and C. D. Easton, *Int. J. Biol. Macromol.*, 2020, **143**, 582–593.
11 M. Tsujiura, D. Ichikawa, S. Komatsu, A. Shiozaki, H. Takeshita and T. Kosuga, *British J. Cancer.*, 2010, **102**, 1174–1179.
12 T. Kilic, A. Erdem, M. Ozsoz and S. Carrara, *Biosens. Bioelectron.*, 2018, **99**, 525–546.
13 L.-L. Zhao, H.-Y. Pan, X.-X. Zhang and Y.-L. Zhou, *Anal. Chim. Acta*, 2020, **116**, 62–69.
14 Y. Peng, J. Jiang and R. Yu, *Anal. Methods*, 2014, **6**, 2889–2893.
15 G. K. Joshi, S. Deitz-McElyea, M. Johnson, S. Mali, M. Korc and R. Sardar, *Nano letters*, 2014, **14**, 6955–6963.
16 Y. Fan, Y. X. Chen, A. D. Trigg, C.-H. Tung, J. Kong and Z. Gao, *J. Am. Chem. Soc.*, 2007, **129**, 5437–5443.
17 P. Jolly, M. R. Batistuti, A. Miodek, P. Zhurauski, M. Mulato, M. A. Lindsay and P. Estrela, *Sci. Rep.*, 2016, **6**, 36719.
18 G.-J. Zhang, J. H. Chua, R.-E. Chee, A. Agarwal and S. M. Wong, *Biosens. Bioelectron.*, 2009, **24**(8), 2504–2508.

19 H.-L. Shuai, K.-J. Huang, W.-J. Zhang, X. Cao and M.-P. Jia, *Sens. Actuators, B*, 2017, **243**, 403–411.
20 M. Moccia, V. Caratelli, S. Cinti, B. Pede, C. Avitabile, M. Saviano, A. L. Imbriani, D. Moscone and F. Arduini, *Biosens. Bioelectron.*, 2020, **165**, 112371.
21 S. Hassanpour, A. Saadati, M. Hasanzadeh, N. Shadjou, A. Mirzaie and A. Jouyban, *Microchim. J.*, 2019, **145**, 266–272.
22 A. Saadati, S. Hassanpour, M. Hasanzadeh, N. Shadjou and A. Hassanzadeh, *Int. J. biol. Macromol.*, 2019, **132**, 748–758.
23 Z. Qiu, J. Shu and D. Tang, *Anal. Chem.*, 2017, **89**, 5152–5160.
24 L. Huang, J. Wang, Q. Wang, D. Tang and Y. Lin, *Microchim. Acta*, 2020, **187**, 563.
25 Z. Yu, Y. Tang, G. Cai, R. Ren and D. Tang, *Anal. Chem.*, 2019, **91**, 1220–1226.
26 A. Saadati, S. Hassanpour, F. Bahavarnia and M. Hasanzadeh, *Anal. Methods*, 2020, **12**, 1639–1649.
27 S. Lv, Y. Tang, K. Zhang and D. Tang, *Anal. Chem.*, 2018, **90**, 14121–14125.
28 Z. Lin, S. Lv, K. Zhang and D. Tang, *J. Mater. Chem. B*, 2017, **5**, 826–833.
29 E. Solhi, M. Hasanzadeh and P. Babaie, *Anal. Methods*, 2020, **12**, 1398–1414.
30 M. Jafari, M. Hasanzadeh, E. Solhi, S. Hassanpour, N. Shadjou, A. Mokhtarzadeh, A. Jouyban and S. Mahboob, *Int. J. biol. Macromol.*, 2019, **126**, 1255–1265.
31 P. Pashazadeh-Panahi, M. Hasanzadeh and R. Eivazzadeh-Keihan, *J. Mol. Recog.*, 2020, **33**, e2828.
32 A. Saeb, A. S. Alshammari, H. Al-Brahim and K. A. Al-Rubeaan, *The Scientific World Journal*, 2014, 2014.
33 Y. Yang, S. Matsubara, M. Nogami, J. Shi and W. Huang, *Nanotechnology*, 2006, **17**, 2821.
34 J. Lu, J. Wang, X. Hu, E. Gyimah, S. Yakubu, K. Wang, X. Wu and Z. Zhang, *Anal. Chem.*, 2019, **91**, 7353–7359.
35 Q. Li, F. Zeng, N. Lyu and J. Liang, *Analyst*, 2018, **143**, 2304–2309.
36 M. Zouari, S. Campuzano, J. M. Pingarrón and N. Raouafi, *ACS omega*, 2018, **3**, 8923–8931.
37 S. S. Low, Y. Pan, D. Ji, Y. Li, Y. Lu, Y. He, Q. Chen and Q. Liu, *Sens. Actuators B: Chem*, 2020, **308**, 127718.
38 S.-R. Ryoo, J. Lee, J. Yeo, H.-K. Na, Y.-K. Kim, H. Jang, J. H. Lee, S. W. Han, Y. Lee and V. N. Kim, *ACS Nano*, 2013, **7**, 5882–5891.
39 Y. Wu, J. Han, P. Xue, R. Xu and Y. Kang, *Nanoscale*, 2015, **7**, 1753–1759.

